minerals

MDPI

*Article*

# Experimental Investigation of Visible-Light and X-ray Emissions during Rock and Mineral Fracture: Role of Electrons Traveling between Fracture Surfaces

**Toshihiko Kadono [1,*], Kazunori Ogawa [2], Kei Shirai [3] Masahiko Arakawa [3], Kosuke Kurosawa [4], Takaya Okamoto [4], Takafumi Matsui [4], Sunao Hasegawa [5], Ayako I. Suzuki [6] and Hideyuki Kobayashi [1]**

[1] Department of Basic Sciences, University of Occupational and Environmental Health, Kitakyusyu 807-8555, Japan; hkobayas@med.uoeh-u.ac.jp
[2] JAXA Space Exploration Center, Japan Aerospace Exploration Agency, Sagamihara 252-5210, Japan; ogawa.kazunori@jaxa.jp
[3] Department of Planetology, Kobe University, Kobe 657-8501, Japan; kei.shirai@penguin.kobe-u.ac.jp (K.S.); masahiko.arakawa@penguin.kobe-u.ac.jp (M.A.)
[4] Planetary Exploration Research Center, Chiba Institute of Technology, Chiba 275-0016, Japan; kosuke.kurosawa@perc.it-chiba.ac.jp (K.K.); tokamoto@perc.it-chiba.ac.jp (T.O.); matsui@perc.it-chiba.ac.jp (T.M.)
[5] Institute of Space and Astronautical Science, Japan Aerospace Exploration Agency, Sagamihara 252-5210, Japan; hasehase@isas.jaxa.jp
[6] Department of Economics, Toyo University, Tokyo 112-8606, Japan; suzuki.ayako.2919@gmail.com
* Correspondence: kadono@med.uoeh-u.ac.jp

## Supplementary Material

### S1. X-ray Data

*S1.1. Original Spectra*

Figure S1a–g show the original X-ray spectra with a bin size of 0.035 keV for (a) quartz by the press, (b) granite by the press, (c) basalt by the press, (d) blank test in the press experiment (metal or plastic shield was placed in front of the detector), (e) granite by the impact, (f) basalt by the impact, and (g) blank shot for granite in the impact experiment (projectile collided the front panel of the target box and did not enter the box).

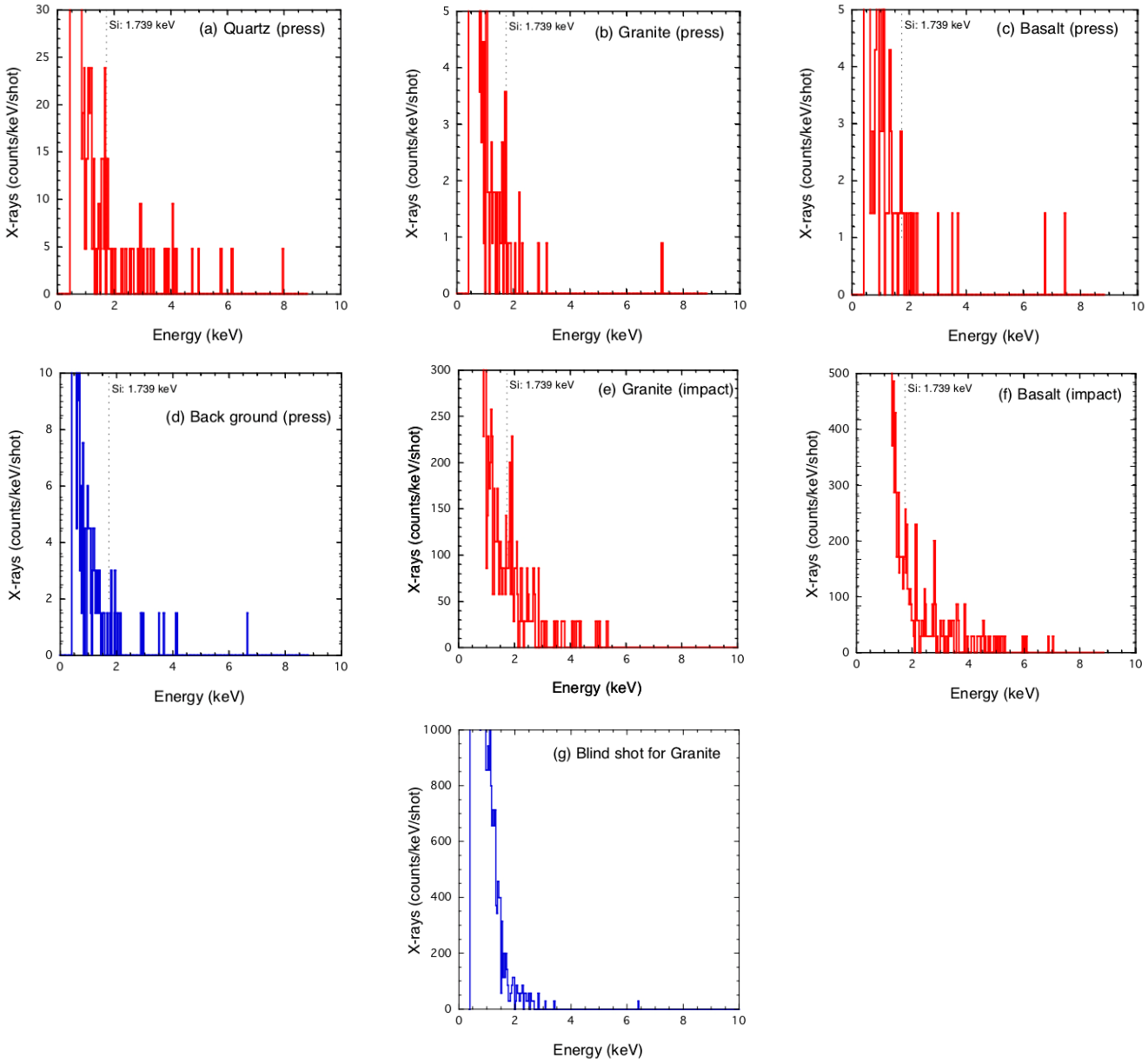


**Figure S1.** X-ray counts (the original data including noise) per bin size (0.035 keV) per shot obtained by the press and impact experiments: (**a**) quartz by the press (the number of shots was 6), (**b**) granite by the press (32 shots), (**c**) basalt by the press (20 shots), (**d**) blank test in the press experiment (19 shots), (**e**) granite by the impact (1 shot), (**f**) basalt by the impact (1 shot), and (**g**) blind shot in the impact experiment (1 shot).

### *S1.2. Peak Around 1.74 keV*

We discuss whether the peak around 1.74 keV in each spectrum is significant or not in comparison to noise (the procedure is schematically described in Figure S2). First, we fit a linear function by the least-squares method to the spectra (with a bin size of 0.035 keV, without background-subtraction, and without normalization by the bin size and the number of shots) between 1.24 keV and 2.24 keV excluding the range around Si line from 1.6 keV to 1.9 keV. Using this function, we calculate the value $\xi$ and deviation $\sigma$ at energy E = 1.739 keV as $\xi = A + B\mathrm{E}$, where $A$ and $B$ are fitting constants, respectively, and $\sigma = (\Delta A^2 + (\mathrm{E}\Delta B)^2)^{1/2}$, where $\Delta A$ and $\Delta B$ are the standard deviations of $A$ and $B$, respectively.

Table S1 shows $\xi$, $\sigma$, $\xi + 3\sigma$, and the peak counts between 1.6 keV and 1.9 keV obtained in the experiments. The peak counts obtained in the experiments for quartz (press), granite

(press), and granite (impact) are larger or comparable with $\xi + 3\sigma$, so it can be said that the possibility that the observed peaks are the Si line is sufficiently certain, while those for basalt (press) and basalt (impact) are ~($\xi + \sigma$) and the possibility seems not sufficiently.

The numbers of shots for quartz and granite (press) are set to obtain a sufficient signal to noise (S/N) ratio (i.e., peak counts ~$\xi + 3\sigma$) while, for basalt, since the S/N ratio did not increase probably because of the lower signal level than the noise level of the detector, the shots were stopped even though the number of shots was less than that for granite. The number of blank shots was set to be the similar to the number of shots for basalt.

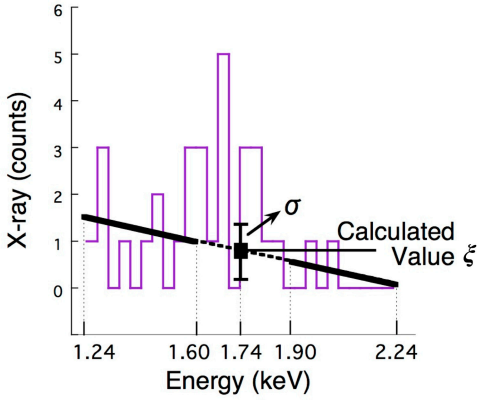


**Figure S2.** Procedure for the evaluation whether the peak around 1.74 keV is the Si line or noise.

**Table S1.** Comparison between peak counts and noise

| Samples | Calculated Value $\xi$ at 1.739 keV Using the Fitting Function | σ at 1.739 keV | $\xi + 3\sigma$ | Peak Counts between 1.6–1.9 keV in the Experiments |
|---|---|---|---|---|
| Quartz (press) | 0.70 | 1.4 | 4.9 | 5 |
| Granite (press) | 0.80 | 1.2 | 4.5 | 4 |
| Basalt (press) | 0.75 | 1.0 | 3.8 | 2 |
| Granite (impact) | 3.1 | 2.0 | 9.0 | 8 |
| Basalt (impact) | 6.8 | 5.3 | 23 | 9 |

*S.1.3. Background Subtraction*

Because the detector is very sensitive for vibration and abrupt temperature change, the disruption experiments, in particular, hypervelocity impacts cause severe environments for the detector. The large components at lower energies should not be X-rays from samples but a noise caused under such environments because Be and polyimide films significantly absorb X-rays at photon energies less than ~1.5 keV. Actually, there are large components at lower energies even in blind shots in impact experiments (e.g., Figure S1g).

As backgrounds, we subtracted the spectrum of the blind shot (the spectra for basalt targets in Figure S1c,f seem to show no clear peak of the Si line and we excluded these data from the subsequent analysis). In the press experiments, the spectrum shown in Figure S1d was subtracted from the spectra obtained by the press (Figure S1a,b). We also subtracted the spectrum of the blind shot in the impact experiments (Figure S1g) from the spectrum obtained by the impact (Figure S1e). In the subtraction, we normalized the total counts in the spectrum of the blind shots in a range of 0.9–1.0 keV with those in the spectrum in the same energy range. The results are shown in Figure 3a–c.

The counts for the press method are assumed to follow a Poisson distribution, and the statistical errors in $N_{pX(Si)}$ and $N_{eX}$ are estimated (there is no statistical error for the impact method because the data is obtained by a single shot).

**S2. Numerical Calculation of X-ray Radiation by Electron Collision**

Counts of fluorescence and bremsstrahlung X-ray photons generated by electron collisions with the samples are estimated using a numerical model for X-ray tubes proposed by Ebel (1999) [28]. We consider the electrons with a monochromatic energy of 3, 5, and 10 keV, colliding with a flat sample surface at an angle of 0 (vertical) and investigate X-ray photons with an emission angle of 0 (vertical to the surface) (Ogawa et al., 2008; Ogawa, 2008) [31,32]. The samples are quartz, granite, and basalt. A model composition of the samples used in the calculations is listed in Table S2. Granite and basalt data are taken from Mason and Moore (1982) [29] and Li (1991) [30]. For granite, we set three cases of X-ray filtering (attenuation): (A) without filtering, (B) polyimide film of 12.5 μm in thickness and the detection efficiency of the Si-PIN detector (i.e., the effects of Be window in front of the detector with 25.4 μm in thickness and Si wafer with 500 μm in thickness as detector) corresponding to the granite disruption in press experiments (Figure 2a), and (C) polyimide film of 37.5 μm in thickness and the same detection efficiency of the Si-PIN detector corresponding to the granite disruption in impact experiments (Figure 2b). For basalt and quartz, we calculate the counts only in the case A (without filtering).

Tables S3–S5 show the numerical results of the X-ray photon counts per steradian from quartz, granite, and basalt, respectively, when $6.25 \times 10^9$ electrons irradiate the sample surface with energies of 3, 5 and 10 keV. Concerning the X-ray counts of the fluorescent lines in the table, only $K_\alpha$ and $K_\beta$ of higher-energy elements are shown, and the counts from C, O and Na and L or the outer-shell lines are omitted. Errors of each X-ray photon count are estimated from errors of physical coefficients in the model, as 20 % for fluorescence counts and 5 % for bremsstrahlung counts at maximum.

The experimental results (Figure 3) show that the lines at higher energies than the Si line (1.7 keV) such as K (3.3 keV) for granite and Ca (3.7 keV) for basalt are unclear. This suggests that the energy of the incident electrons is expected to be less than ~5 keV, as shown in the numerical results for electron energies of 5 and 10 keV in the case C indicating that the counts per steradian at the K or Ca lines are comparable or higher than those at the Si line (e.g., Table S4). The counts per steradian at the Si line $N$ at an electron energy of 3 keV is $2.8 \times 10^4$ counts/sr (quartz), $2.1 \times 10^4$ counts/sr (granite), and $1.5 \times 10^4$ counts/sr (basalt) in the case A (without filtering) for each sample (Tables S3–S5), and we obtain the number of photons at every direction $4\pi N$. Therefore, the efficiency $\eta$ can be obtained by normalizing $4\pi N$ by the number of incident electrons $6.25 \times 10^9$ as $5.6 \times 10^{-5}$ for quartz, $4.2 \times 10^{-5}$ for granite, and $3.0 \times 10^{-5}$ for basalt.

As shown in the Section 3.1., the total number of the X-rays $N_{pX(Si)}$ at the energy of the Si line in every direction is estimated as $(5.6 \pm 1.7) \times 10^5$ and $(8.7 \pm 3.5) \times 10^4$ photons/cm$^2$ for quartz and granite during press disruption, and $2.9 \times 10^5$ photons/cm$^2$ for granite target during impact disruption. Thus, the number of electrons in every direction $N_{eX} = N_{pX(Si)}/\eta$ is $(9.9 \pm 2.9) \times 10^9$ and $(2.1 \pm 0.8) \times 10^9$ electrons/cm$^2$ for quartz and granite during press disruption, and $6.9 \times 10^9$ electrons/cm$^2$ for granite target during impact disruption.

**Table S2.** A model composition of the samples in mass fraction.

| Element | Quartz | Granite | Diabase (basalt) |
|---|---|---|---|
| C | | 0.20 | 0.01 |
| O | 53.30 | 45.50 | 44.90 |
| Na | | 2.46 | 1.60 |
| Mg | | 0.24 | 3.99 |
| Al | | 7.43 | 7.94 |
| Si | 46.70 | 33.96 | 24.61 |
| K | | 4.51 | 0.53 |
| Ca | | 0.99 | 7.83 |

| | | | |
|---|---|---|---|
| Ti | | 0.15 | 0.64 |
| Mn | | 0.20 | 0.13 |
| Fe | | 1.37 | 7.76 |
| Total | 100.00 | 97.01 | 99.94 |

**Table S3.** Quartz: The calculation result of fluorescence and bremsstrahlung X-ray photon counts per steradian from quartz at an emission angle of 0, when $6.25 \times 10^9$ electrons perpendicularly irradiate target surface.

| **Electron Acceleration Voltage** | **3 kV** | **5 kV** | **10 kV** |
|---|---|---|---|
| **Filtering** | **A** | **A** | **A** |
| Bremsstrahlung Total | 81,968 | 149,138 | 315,723 |
| Mg K$\alpha$ (1.25 keV) | 0 | 0 | 0 |
| Al K$\alpha$ (1.49 keV) | 0 | 0 | 0 |
| Al K$\beta$ (1.55 keV) | 0 | 0 | 0 |
| Si K$\alpha$ (1.74 keV) | 28,144 | 145,066 | 560,699 |
| Si K$\beta$ (1.84 keV) | 484 | 2497 | 9711 |
| K K$\alpha$ (3.31 keV) | 0 | 0 | 0 |
| K K$\beta$ (3.59 keV) | 0 | 0 | 0 |
| Ca K$\alpha$ (3.69 keV) | 0 | 0 | 0 |
| Ca K$\beta$ (4.01 keV) | 0 | 0 | 0 |
| Fe K$\alpha$ (6.40 keV) | 0 | 0 | 0 |
| Fe K$\beta$ (7.06 keV) | 0 | 0 | 0 |

**Table S4.** Granite: The calculation result of fluorescence and bremsstrahlung X-ray photon counts per steradian from granite.

| **Electron Acceleration Voltage** | **3 kV** | | | **5 kV** | | | **10 kV** | | |
|---|---|---|---|---|---|---|---|---|---|
| **Filtering** | **A** | **B** | **C** | **A** | **B** | **C** | **A** | **B** | **C** |
| Bremsstrahlung Total | 87,052 | 3336 | 984 | 157,874 | 20,099 | 10,577 | 330,991 | 106,287 | 75,830 |
| Mg K$\alpha$ (1.25 keV) | 365 | 9 | 0 | 1167 | 28 | 0 | 3407 | 81 | 1 |
| Al K$\alpha$ (1.49 keV) | 7695 | 784 | 39 | 30112 | 3069 | 152 | 100937 | 10288 | 508 |
| Al K$\beta$ (1.55 keV) | 46 | 6 | 0 | 181 | 24 | 2 | 611 | 82 | 6 |
| Si K$\alpha$ (1.74 keV) | 21,050 | 4956 | 726 | 107,973 | 25,420 | 3723 | 409,145 | 96,324 | 14,110 |
| Si K$\beta$ (1.84 keV) | 362 | 105 | 20 | 1860 | 540 | 104 | 7111 | 2065 | 398 |
| K K$\alpha$ (3.31 keV) | 0 | 0 | 0 | 1964 | 1584 | 1179 | 25,156 | 20,292 | 15,098 |
| K K$\beta$ (3.59 keV) | 0 | 0 | 0 | 183 | 155 | 123 | 2359 | 1995 | 1582 |
| Ca K$\alpha$ (3.69 keV) | 0 | 0 | 0 | 192 | 164 | 133 | 4517 | 3871 | 3128 |
| Ca K$\beta$ (4.01 keV) | 0 | 0 | 0 | 20 | 18 | 15 | 474 | 421 | 357 |
| Fe K$\alpha$ (6.40 keV) | 0 | 0 | 0 | 0 | 0 | 0 | 1002 | 973 | 934 |
| Fe K$\beta$ (7.06 keV) | 0 | 0 | 0 | 0 | 0 | 0 | 120 | 117 | 114 |

**Table S5.** Basalt: The calculation result of fluorescence and bremsstrahlung X-ray photon counts per steradian from basalt (diabase).

| **Electron Acceleration Voltage** | **3 kV** | **5 kV** | **10 kV** |
|---|---|---|---|
| **Filtering** | **A** | **A** | **A** |
| Bremsstrahlung Total | 95381 | 172909 | 358285 |
| Mg K$\alpha$ (1.25 keV) | 5869 | 18714 | 53747 |
| Al K$\alpha$ (1.49 keV) | 7959 | 30987 | 101753 |
| Al K$\beta$ (1.55 keV) | 48 | 186 | 618 |
| Si K$\alpha$ (1.74 keV) | 14781 | 75553 | 282320 |
| Si K$\beta$ (1.84 keV) | 254 | 1303 | 4920 |
| K K$\alpha$ (3.31 keV) | 0 | 224 | 2876 |
| K K$\beta$ (3.59 keV) | 0 | 21 | 270 |
| Ca K$\alpha$ (3.69 keV) | 0 | 1474 | 34850 |
| Ca K$\beta$ (4.01 keV) | 0 | 154 | 3654 |
| Fe K$\alpha$ (6.40 keV) | 0 | 0 | 5506 |
| Fe K$\beta$ (7.06 keV) | 0 | 0 | 660 |

## S3. The Results of Visible Light

We observed the visible-light emission during fracture with a photo-multiplier and an imaging camera in the press experiments in the atmosphere. The outputs of the photo-multiplier and the images of the original samples and light emissions taken by the camera are shown in Figures S3 and S4 for quartz, Figures S5 and S6 for granite and Figure S7 for basalt (no image was obtained for basalt by the imaging camera). An arrow indicates the position of light emission when the area is small. Figure S8 shows the outputs of the photo-multiplier with quartz and granite placed between polyvinyl chloride plates.

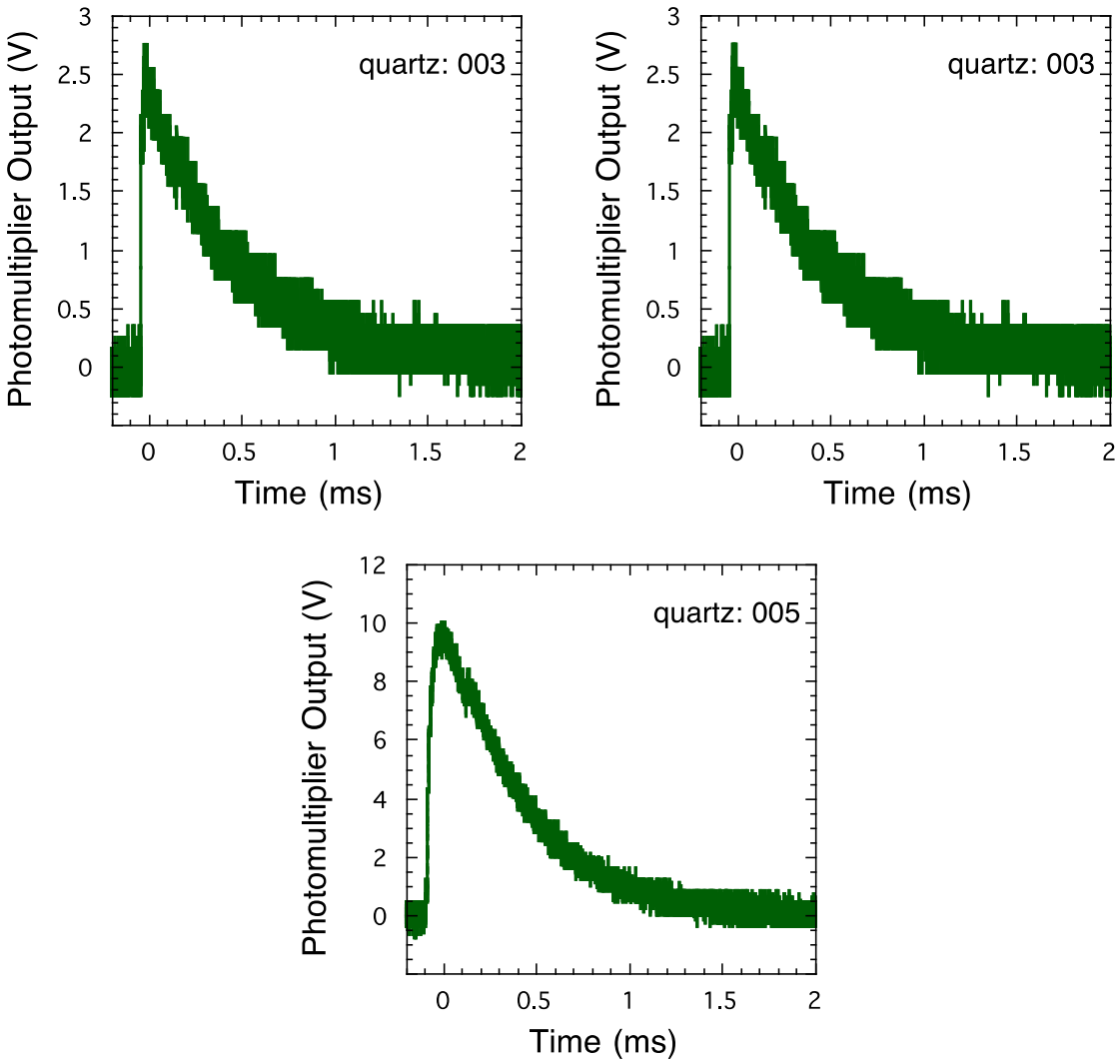


**Figure S3.** Photomultiplier output for quartz. The result named quartz 005 is the same as Figure 4a. The light was too intense in quartz 004 and the peak voltage was not be obtained.

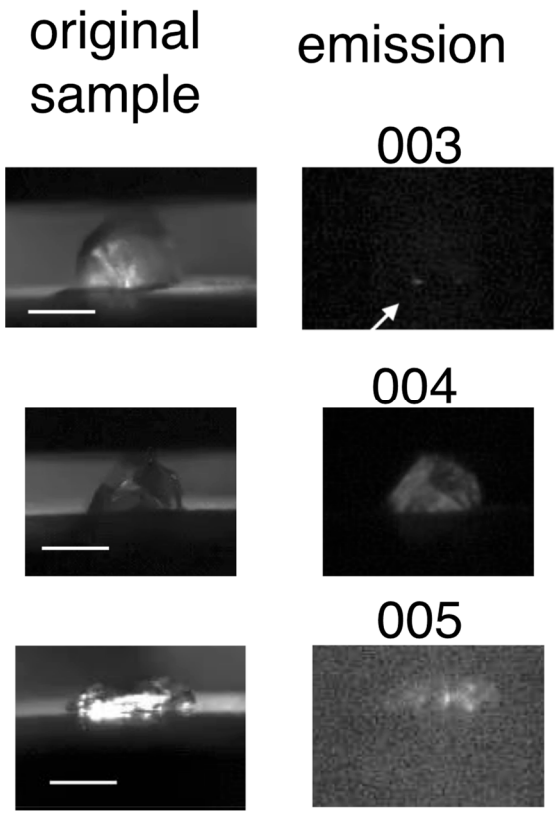


**Figure S4.** Quartz sample images before fracture (upper line) and the light emission during fracture (lower line). Number 005 is the same as the images in Figure 4a. The horizontal white bar in each figure of the original sample indicates 1 cm.

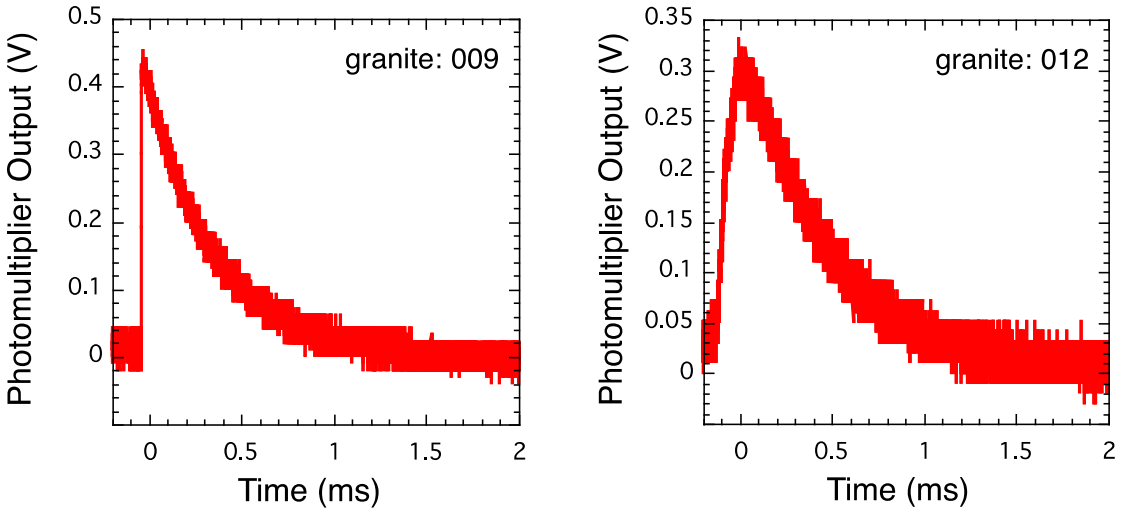

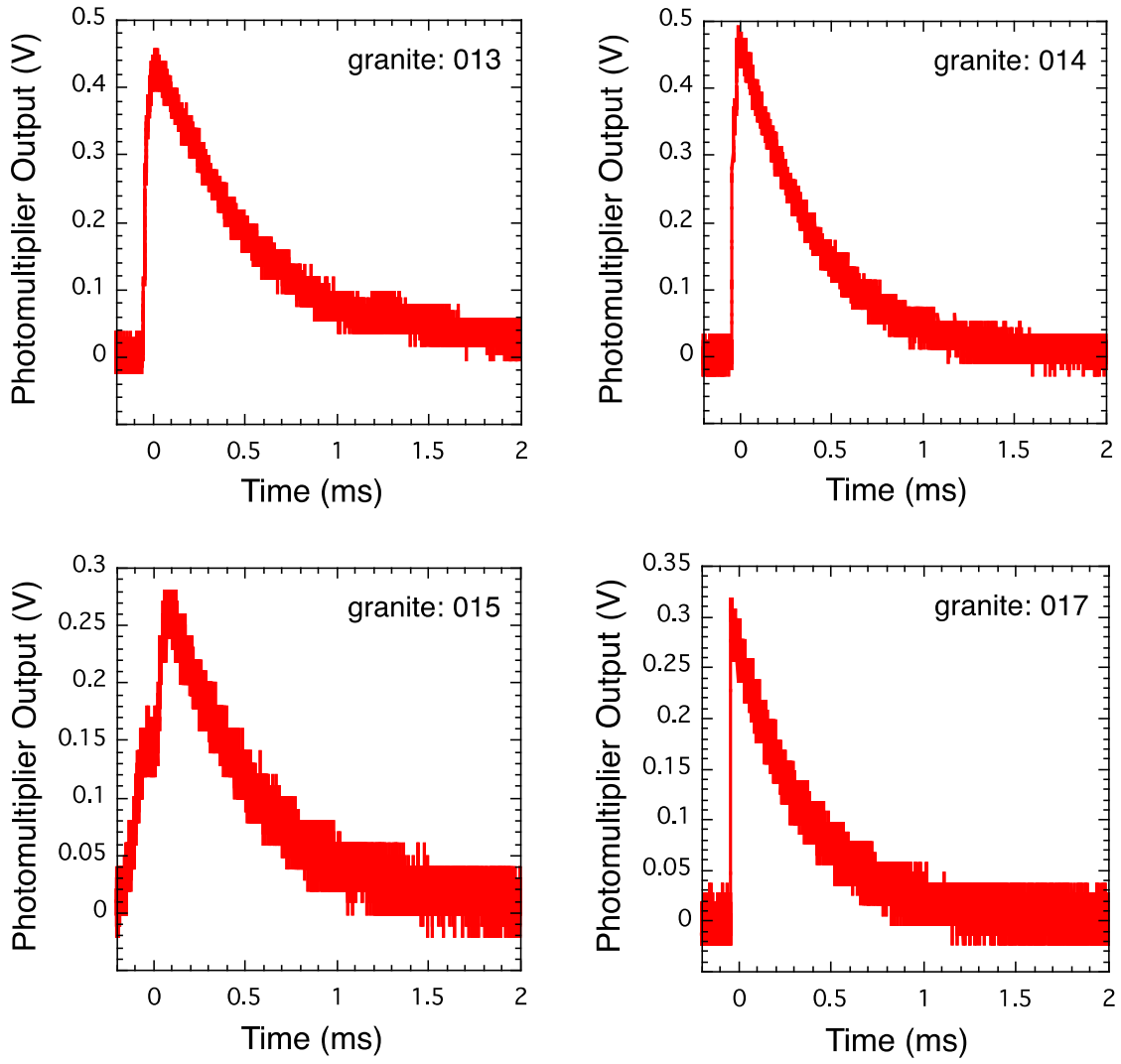


**Figure S5.** Photomultiplier output for granite. The result of granite 009 is the same as Figure 4b.

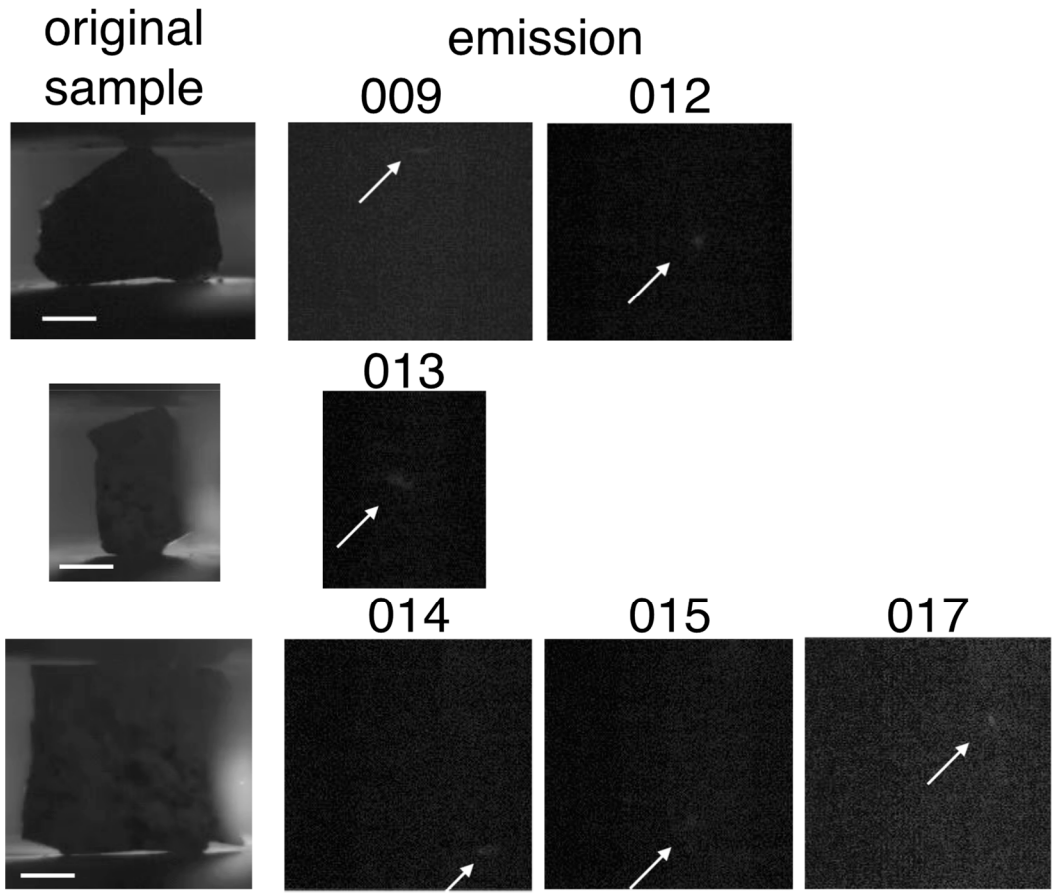


**Figure S6.** Granite sample images before fracture (left-end in each line) and the light emission during fracture (denoted by the number). Number 009 is the same as the image in Figure 4b. The horizontal white scale bar indicates 1 cm in each image before fracture. When the samples emitted the light, sometimes they were partially (not completely) broken. In this case, we continued to press the samples until next emission. For the sample shown in the third line, we observed the light emissions three times (014, 015 and 017).

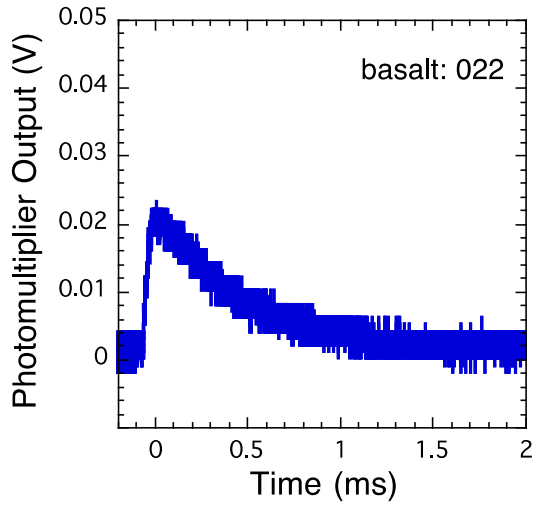


**Figure S7.** Photomultiplier output for basalt (the same as Figure 4c). No image was obtained by the camera.

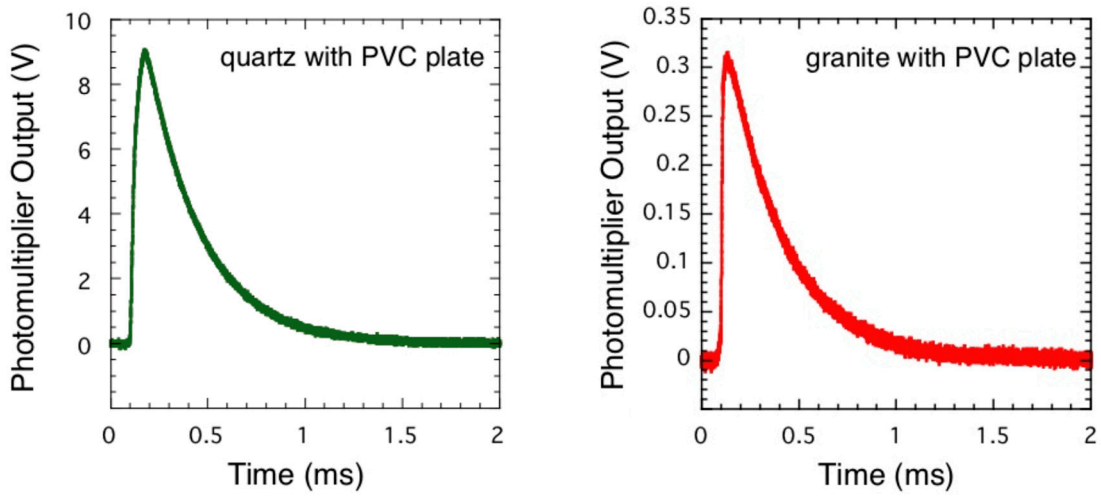


**Figure S8.** Photomultiplier output for quartz and granite placed between polyvinyl chloride plates.

## References in the section S2

1. Ebel, H. X-ray tube spectra. *X-ray Spectrom.* **1999**, *28*, 255–266.
2. Li, Y.-H. Distribution patterns of the elements in the ocean: A synthesis. *Geochim. Cosmochim. Acta* **1999**, *55*, 3223–3240.
3. Mason, B.; Moore, C.B. *Principles of Geochemistry*, 4th ed.; John and Wiley & Sons: New York, NY, USA, 1982.
4. Ogawa, K. Basic Development of a Compact X-ray Tube for In-Situ X-ray Analysis of Planetary Surface Composition. Ph.D. Thesis, Tokyo Institute of Technology, Tokyo, Japan, 2008.
5. Ogawa, K.; Okada, T.; Shirai, K.; Kato, M. Numerical estimation of lunar X-ray emission for X-ray spectrometer onboard SELENE. *Earth Planets Space* **2008**, *60*, 283–292.